

Jamming on deformable surfaces

Zhaoyu Xie and Timothy J. Atherton

Tufts University, Dept. of Physics & Astronomy, 574 Boston Ave, Medford, MA 02155

Jamming is a fundamental transition that governs the mechanical behavior of particulate media, including sand, foam and dense suspensions but also biological tissues: Upon compression, particulate media can change from freely flowing to a disordered solid. Jamming has previously been conceived as a bulk phenomenon involving particle motions in fixed geometries. In a diverse class of soft materials, however, solidification can take place in a deformable geometry, such as on the surface of a fluid droplet or in the formation of a bijel. In these systems the nature and dynamics of jamming remains unknown. Here we propose and study a scenario we call metric jamming that aims to capture the complex interactions between shape and particles. Unlike classical jamming processes that exhibit discrete mechanical transitions, surprisingly we find that metric jammed states possess mechanical properties that are continuously tunable between those of classical jammed and conventional elastic media. New types of vibrational mode that couple particulate and surface degrees of freedom are also observed. Our work lays the groundwork for a unified understanding of jamming in deformable geometries, to exploit jamming for the control and stabilization of shape in self-assembly processes, and provides new tools to interrogate solidification processes in deformable media more generally.

Jamming is a transition to rigidity that occurs as particulate media are compressed from a freely flowing state to a solid state[1, 2]. Jamming can be induced by varying thermodynamic variables such as temperature and density, as well as mechanical variables such as applied stress: Colloidal suspensions become colloidal glasses as the density is increased, flowing foams become static as the shear stress is decreased below yield stress, liquids become glasses as the temperature is lowered below the glass transition[3, 4]. Moreover, in biological systems, confluent tissues also exhibit a transition to rigidity controlled by single-cell properties such as shape and motility[5–8].

Recently, however, a number of experiments have emerged that involve solidification in deformable geometries and do not neatly fit into the jamming scenarios previously envisioned because these only consider particle-particle interactions and take place in Euclidean space with a fixed geometry. In these new situations, the rigidification takes place not only with respect to particle degrees of freedom, but also with respect to the shape of the interface itself. Further, the non-Euclidean geometry of the interface means that particles in different locations may experience location dependent states of stress depending on the local shape of the interface.

In this work, we therefore propose a new jamming class, which we refer to as *metric jamming*, that refers to structures jammed both with respect to particle degrees of freedom and surface degrees of freedom. The purpose of this paper is to construct a model metric jamming process, explicitly test the resulting structures for rigidity and hence distinguish similarities and differences from other jammed media.

The jammed state has unique properties compared to normal crystalline solids and new physics emerges near the jamming transition[1, 4]. In contrast to crystalline solids, jammed materials generally lack translational order and are fragile, offering little or no resistance to shear

deformation, and exhibit other unusual elastic properties if the particles themselves are deformable. The fragility arises from the packing’s *isostaticity*, i.e. they possess only the minimal number of contacts per particle required for mechanical stability. Understanding jamming of disordered systems will help the fabrication of new functional amorphous materials[9–11].

Jamming theory has been extended to consider nonspherical[12, 13] and deformable [14, 15] particles as well as the role of friction[16]. In such extensions, both *hypostatic* and *hyperstatic* configurations—those with an apparent deficit or surplus of contacts relative to the isostatic value—can emerge requiring sophisticated approaches to constraint counting[17, 18] and new universality classes[19].

Two distinct theoretical approaches to jamming have been proposed: One considers jammed states of soft particles that interact via a short range interparticle potential $V(r)$ [4]. The energy of the system is expanded as a quadratic form $U \sim \delta x \cdot H \cdot \delta x$ about a candidate jammed state of interest, where H is the Hessian matrix of the energy, also known as dynamical matrix[20–22], and δx is the displacement vector. Eigenanalysis of H is used to test the overall stability of the structure, and hence if it is truly jammed, identify particles (known as *rattlers*) that are superfluous to the rigidity. The spectrum of H also provides the density of vibrational states and therefore determines the elastic response. Jammed structures are found to possess an excess of low-frequency modes that are a signature of the fragility of the state[4, 20–29].

An alternative approach considers configurations of rigid, mutually impenetrable particles under confinement[30]. Particles in a candidate structure are subjected to set of random forces ξ to find a prototypical unjamming motion δx identified by extremization of the virtual work $\xi \cdot \delta x$, a linear programming problem, subject to (linearized) interpenetrability constraints[31, 32]. Analysis of the prototypical un-

jamming motion leads to a hierarchical classification of jammed structures[33]: A packing is *locally jammed*, the least stringent category, if no particles are able to move while the others remain fixed; it is *collectively jammed* if no subset of particles is movable with the remainder held in place; it is *strictly jammed* if no collective subset of the particles can be moved at the same time as a volume conserving deformation of the container.

Examples of solidification in deformable geometries include the phenomenon of arrested coalescence in Pickering emulsions[34], mixtures of immiscible fluids stabilized by the addition of colloidal particles adsorbed at the fluid-fluid interface of the constituent droplets. Here, emulsion droplets successively coalesce, leading to gradual densification of the particles and, ultimately, rigid arrested structures that inhibit further coalescence. Deformation of Pickering emulsion droplets by an electric field can rigidify in wrinkled patterns[35]. Another example involves colloidal particles immersed in a host fluid that undergoes a phase transition to a liquid crystalline phase; the moving phase boundary drives the particles to remain in the vanishing isotropic phase which densify and jam forming rigid shells[36]. Other situations involve more exotic particles, such as bacteria on the interface of an oil-in-water emulsion droplet that they gradually consume[37], or non-compact interfaces, such as the production of jammed emulsion gels (bijels) from bicontinuous precursor mixtures[38, 39].

MODEL SYSTEM

To do so, we consider the following simplified scenario: suppose N soft spherical frictionless particles with different radii r_i are positioned with their centroids at coordinates \mathbf{X}_i on a closed compact surface ∂C that bounds a region C of fixed volume representing, for example, an emulsion droplet. To facilitate comparisons with studies of jamming in flat space[4, 26, 40–45], we will use 50–50 mixtures of bidispersed particles with radius ratio 1 : 1.4 to suppress crystallization. For simplicity, we assume that the particles are rigidly confined to the surface and that their presence does not significantly deform the interface locally by forming menisci. The particles interact with one another through a potential of finite range $V(d_{ij})$ where d_{ij} is the separation of particles i and j .

The total energy of the system includes both surface tension and particle-particle interactions,

$$E = \sigma \int dA + k \sum_{i \neq j} V(d_{ij}), \quad (1)$$

where σ is the surface tension and k is the rigidity of the particles. A dimensionless ratio $K = \sigma A/k$ characterizes the relative importance of these terms where A is the surface area. The choice of surface energy here is specific to the Pickering emulsion scenario described above: The

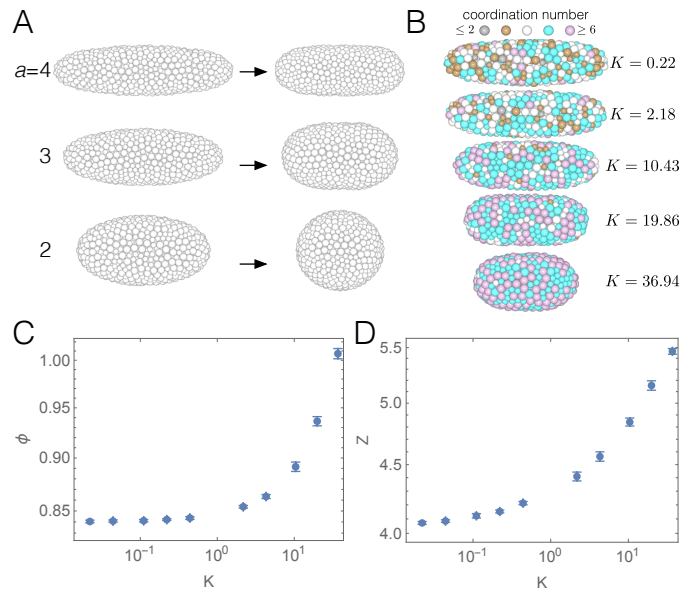


Figure 1. **Metric jammed configurations.** **A** Initially jammed configurations on ellipsoids of varying aspect ratio (left) are relaxed into metric jammed structures (right). **B** Final metric jammed configurations as a function of K . **C** Packing fraction as a function of K . **D** Mean contact number per particle as a function of K .

integral in (1) is over the exposed fluid-fluid interface of the emulsion droplet which might be locally deformed due to capillary effects. For simplicity, we will here assume that the particles each occupy a fixed interfacial area and instead integrate over the area of the whole surface, supplementing (1) with a constant $-\sum_i \pi r_i^2$ that does not enter into our later calculations where r_i is the radius of a single particle. Other surface energies might be applicable in different scenarios, e.g. the Helfrich energy for jamming on a vesicle[46], for example, or an elastic energy for a membrane.

The surface is parameterized by a map $\mathbf{X}(\mathbf{x}) = \mathbf{x}R(\mathbf{x})$ from points \mathbf{x} that lie on the unit sphere to 3D Euclidean space where the radial function $R(\mathbf{x})$ is decomposed into tesseral harmonics,

$$R(c_{lm}, \mathbf{x}) = \sum_{lm} c_{lm} Z_{lm}(\mathbf{x}). \quad (2)$$

The configuration of the system may be fully specified by the set of parameters $\xi = \{\mathbf{x}_i, c_{lm}\}$ including N particle positions \mathbf{x}_i on the unit sphere and M surface coefficients c_{lm} for a total of $2N + M$ degrees of freedom. Fixing the volume enclosed by the surface imposes a nonlinear constraint on the surface coefficients $\{c_{lm}\}$ and removes one degree of freedom. The physical position \mathbf{X}_i of the i th particle may be calculated from the map \mathbf{X} and depends on \mathbf{x}_i and $\{c_{lm}\}$.

For particle-particle interactions we use a compact repulsive pairwise potential[4, 21, 22, 25, 40–45, 47, 48],

$$V(d_{ij}) = \frac{1}{2} \left(1 - \frac{d_{ij}}{s_{ij}}\right)^2 \Theta \left(\frac{d_{ij}}{s_{ij}} - 1\right), \quad (3)$$

where the separation $d_{ij} = |\mathbf{X}_i - \mathbf{X}_j|$, $s_{ij} = r_i + r_j$ and Θ is the Heaviside step function enforcing interaction only for overlapping particles.

SIMULATIONS

We construct metric jammed configurations by the following procedure: we first create rigid packings on surfaces of fixed shape, specifically ellipsoids of varying aspect ratio. These will be used to help distinguish the physical consequences of the curved geometry from those associated with the surface modes. Using the ellipsoidal packings as a starting point, we then minimize the total energy (1) of the configuration with respect to both particle and surface parameters ξ , producing a final jammed structure. Further details are provided in the Methods section below. Fig. 1A displays initial and final states for several different aspect ratios. In the majority of the paper, we use $N = 800$ particles, a figure large enough to mitigate finite size effects but sufficiently small for computational expediency.

For each configuration, the stability is assessed by calculating and diagonalizing the bordered hessian of the energy functional (1) with respect to the parameter set ξ incorporating both particle and surface degrees of freedom and including the volume constraint. Particle coordinates are parametrized in spherical polar form $\mathbf{x}_i = R(\sin \theta_i \cos \phi_i, \sin \theta_i \sin \phi_i, \cos \theta_i)$. Rattlers, particles that do not contribute to the rigidity of the structure, are identified from zero modes of the hessian associated with eigenvectors that are localized to a single particle; these particles are then removed from the structure. There also exist zero modes associated with residual degrees of freedom; for ellipsoids there is one such mode associated with cylindrical symmetry about the long axis; for spherical packings there are three. In practice, the zero modes arising from numerical calculations mix combinations of rattler and trivial motions which must be separated by Gram-Schmidt orthogonalization of the associated eigenvectors.

STRUCTURAL ANALYSIS

Metric jammed structures for different values of K for $N = 800$ particles are shown in Fig. (1)B. For large K , with large surface tension, the final shape tends towards spherical, and hence achieves a globally minimal surface; for smaller K , or larger inter-particle interaction energies, the shape instead tends toward spherocylindrical. From these, we can compute two structural measures, the packing fraction $\phi = (N\pi/A) \sum_i r_i^2$, where A is the

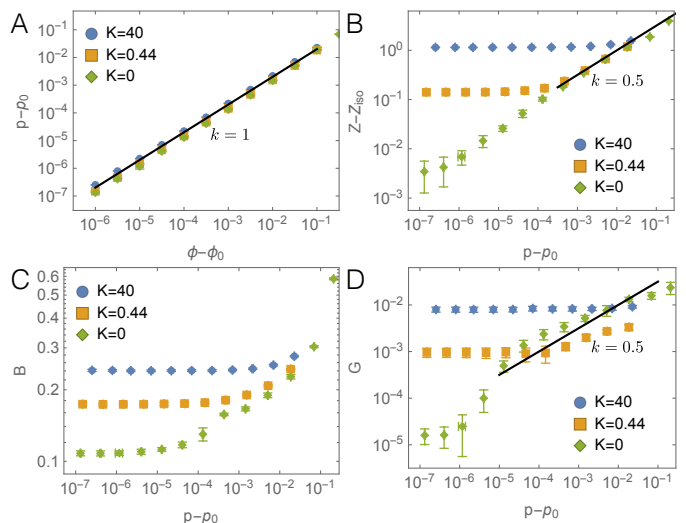


Figure 2. **Mechanical properties of metric jammed configurations.** (a) Relation between pressure and packing fraction. (b) change in contact number as a function of pressure. Elastic moduli as a function of pressure for different K : (c) bulk modulus and (d) shear modulus.

area of the surface at the jamming point, and the mean number of contacts per particle Z , that are signatures of jamming in flat space. Fig. (1)C displays ϕ as a function of K for $N = 400$ particles: As $K \rightarrow 0$, ϕ approaches the value of 0.84 characteristic of random close packing in 2D space[4]. As K increases, the particles are increasingly compressed and the exposed surface gradually eliminated hence $\phi \rightarrow 1$ for large K . The mean contact number Z is plotted with respect to K in Fig. (1)D also for $N = 400$ particles and tends towards 4 as $K \rightarrow 0$ which for $K \rightarrow 10$ the number of contacts is significantly greater, reaching values as high as 5.5.

We now compare these results with the situation in flat space. A linear constraint counting argument predicts the minimal number of contacts: the number of degrees of freedom for N particles is dN where d is the dimensionality and ξ is the number of residual degrees of freedom in the space ($\xi = d$ in d -dimensional space and $\xi = 1$ for cylindrically symmetric surfaces as discussed above). These must be balanced by $NZ_{iso}/2$ constraints, i.e. $dN = NZ_{iso}/2 + \xi$. The isostatic contact number in 2D is therefore $Z_{iso} = 4 - 4/N$. Previous literature demonstrates that an additional degree of freedom is required to maintain positive pressure and bulk modulus in flat space, such that $dN + 1 = NZ_c + \xi$ [43, 49]. Thus the contact number at jammed state $Z_c = 4 - 2/N$ on 2D flat surfaces and $Z_c = 4$ on cylindrically symmetric surfaces. Hence, the metric jammed structures produced are generally *hyperstatic* and reproduce the isostaticity observed in flat space only as $K \ll 1$, i.e. where the rigidity of the particles is significantly greater than the surface tension. In that limit, the packing fraction approaches the random close packing value.

MECHANICAL PROPERTIES

Jammed structures in 2D flat space also exhibit a unique elastic response: they possess vanishing shear modulus, and exhibit characteristic scalings of the pressure $p \sim (\phi - \phi_0)^1$, excess contact number $\Delta Z \equiv Z - Z_{iso} \sim (\phi - \phi_0)^{1/2}$, bulk and shear elastic moduli $B \sim (\phi - \phi_0)^0$, $G \sim (\phi - \phi_0)^{1/2}$ as the system is compressed beyond the jamming point ϕ_0 [2, 4, 43, 49]. To test this, we deform metric jammed configurations in two ways: the structure is compressed slightly to measure the bulk modulus B and a twist deformation is imposed about the symmetry axis to measure the shear modulus G . The elastic moduli are computed from derivatives of the stress tensor during the deformation as described in Methods and results for packings with different K are displayed in Fig. 2.

Fig. 2(a), shows that the excess pressure $\Delta p = p - p_0$ is proportional to the excess packing fraction $\phi - \phi_0$ and is therefore a good measure of the deformed system's proximity to the jamming point. The excess contact number, bulk modulus and shear modulus are displayed as a function of Δp in Fig. 2(b)-(d). The excess coordination number displays an initial plateau but then increases at a critical pressure that increases with K . Far from the jamming point, the excess contact number scales as $\Delta Z \sim (\Delta p)^{0.5}$. The bulk modulus possesses a similar plateau for all K at low Δp . The shear modulus G is several orders of magnitude smaller than the bulk modulus, and increases approximately proportionally to K . For small K , G scales approximately like $(\Delta p)^{0.5}$; this behavior is reproduced for larger K only at higher pressure where a plateau exists for small Δp . Hence, these results well reproduce the behavior of jammed packings in flat space at low K . As $K \gg 1$, the structures begin to resemble normal solids where $G \sim (\phi - \phi_c)^0$ [2, 4, 43, 49] even though G remains small.

VIBRATIONAL MODES

A third signature of the jammed state is an excess of low frequency vibrational modes[4, 20–22, 24–27, 29, 50, 51], in contrast to the Debye theory of elastic solids[52, 53]. Eigenanalysis of the hessian matrix provides the vibrational frequencies, which are the square roots of the eigenvalues measured in units of \sqrt{k}/r where r is the radius of the larger particle, and associated vibrational modes from the eigenvectors. We display the density of states $D(\omega)$ for different values of K in Fig. 3A at several values of $\Delta\phi = \phi - \phi_0$. Two key features are apparent: first, $D(\omega)$ possesses a low frequency plateau characteristic of jamming for low K and at low $\Delta\phi$. As the system is compressed, or as K increases, the plateau vanishes leading to Debye-like behavior.

A second feature is that $D(\omega)$ falls abruptly above a critical value of ω . The transition is very sharp as $K \rightarrow 0$ and smoothed out for larger K . In Fig. 3B, we display

the component of the eigenvectors in the polar direction as a function of ω , close to the metric jammed configuration. At low frequency, particles tend to vibrate along the azimuthal ϕ direction while high-frequency localized vibrations are along the polar θ direction. The crossover of $D(\omega)$ coincides with the transition of particle motions. For packings on spherical surfaces the high frequencies have motions both along θ and ϕ directions due to the symmetric nature. Hence spatially inhomogeneous curvature can cause the localization of vibrational modes.

The participation ratio $P(\omega)$ is calculated to characterize the vibrational modes[22, 24, 29, 47, 50]. It is a measure of the fraction of particles that are participating in the motion governed by the mode of frequency ω . Given the eigenvectors $\{\vec{u}_i(\omega)\}$ at frequency ω for every particle,

$$P(\omega) = \frac{1}{N} \frac{(\sum_i |u_i(\omega)|^2)^2}{\sum_i |u_i(\omega)|^4}, \quad (4)$$

where N is the number of particles after removing ratters. On the curved surfaces considered here, we use the arclength to represent $|u_i(\omega)|^2$.

The corresponding participation ratios $P(\omega)$ are also displayed in Fig. 3C together with illustrations of typical vibrational modes in Fig. 3D for configurations close to the metric jamming point with $K = 40$, revealing the consequences of anisotropic curvature. In the low-frequency region far from the jamming point, plane-wave like phonon modes (Fig. 3D ii) and quasi-localized modes (Fig. 3D iii) where localized excitations are visible on a small plane-wave background. In the mid-frequency region, we have extended modes where random excitations spread throughout the entire system along the azimuthal ϕ direction (Fig. 3D iv), and along the polar θ direction (Fig. 3D v) for larger frequencies. The high-frequency region contains localized modes where only a few particles vibrate along the polar θ direction (Fig. 3D vi). These vibrational modes also exists for jammed structures on flat surfaces[1, 2, 26, 29, 50, 54]. The spatially inhomogeneous curvature, however, causes the extended modes along the polar θ or azimuthal ϕ direction. Additionally for metric jammed configurations at very low frequency where the component of eigenvectors along θ direction and participation ratio are almost 1, there appears a vibrational mode where all particles move along the θ direction, showed in Fig. 3i.

Our inclusion of shape as well as particulate degrees of freedom allows for the possibility of new modes with mixed character. To examine this, we display in Fig. 4A and B the projection of each normalized eigenvector that lies in the shape sector, $c(\omega)$, as a function of the angular frequency. We see that modes associate with significant shape deformation tend to lie in the high frequency regime, relatively independently of K . Two such modes are depicted in Fig. 4C and D.

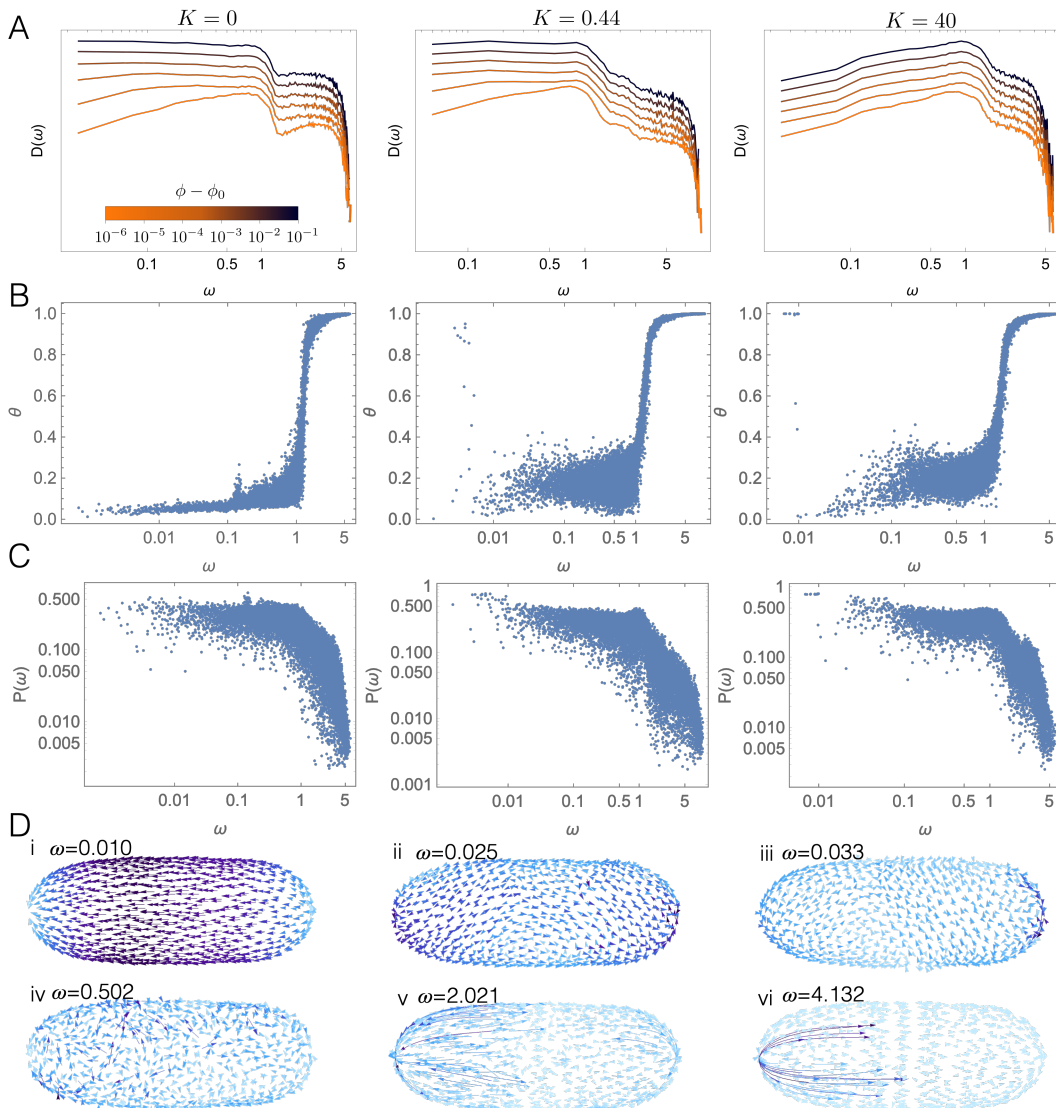


Figure 3. **Vibrational properties of metric jammed configurations.** **A** Vibrational density of states $D(\omega)$, **B** vibrational component along polar axis for $\phi - \phi_0 = 10^{-6}$ and **C** participation ratio $P(\omega)$ for metric jammed configuration with $K = 0$, $K = 0.44$ and $K = 40$ at $\phi - \phi_0 = 10^{-6}$. **D** Selected vibrational modes for $K = 40$: **i** translation along polar direction, **ii** phonon mode, **iii** quasi-localized mode, **iv** extended mode along polar direction, **v** extended mode along azimuthal direction, **vi** localized mode.

CONCLUSION

These results collectively show that particulate media on deformable surfaces can form structures that share structural and mechanical properties with conventional jammed media in Euclidean space, but are rigid with respect to surface as well as particle degrees of freedom. Experimentally produced structures are likely to initially be arrested, i.e. only locally jammed, but by successive unjamming and relaxation events proceed toward a new *metric jammed* state that is rigid with respect to surface as well as particle degrees of freedom. The presence of a surface energy tends to compress the particles somewhat in the final state, and hence metric jammed structures

resemble those in flat space only in the limit of high particle rigidity. By adjusting the relative influence of surface and particle energies characterized by a single dimensionless parameter $K = \sigma A/k$, metric jammed structures can continuously be tuned from isostatic with vanishing shear modulus, i.e. similar to jammed states in flat space, to states that resemble conventional elastic solids. A simple structural metric, the coordination number, serves as an indicator of where in this range a particular candidate structure lies. The vibrational spectrum may similarly be tuned from similar to a jammed solid, possessing an excess of low frequency modes, to Debye-like. In either case, the curved space leaves a significant imprint on the spectrum, leading to localized and oriented modes due to

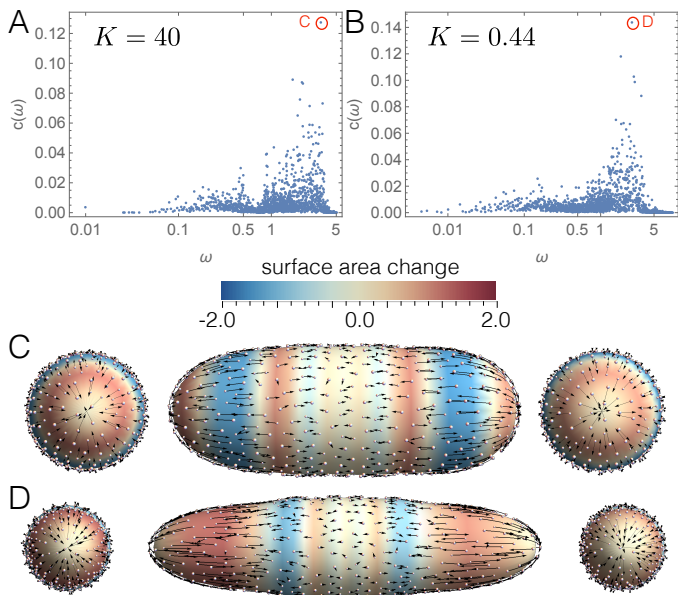


Figure 4. **Combined shape-particle vibrational modes.** **A** Projection $c(\omega)$ of the eigenvector associated with the shape deformation sector for rigid particles $K = 40$ and **B** $K = 0.44$. **C** and **D** Representative eigenvectors with significant shape and particle deformation; the local rate of change in area is plotted together with arrows indicating particle motions.

the anisotropic curvature.

Our work provides a theoretical framework that unifies our understanding of solidification processes that take place on deformable media and extends the applicability of the jamming concept. Beyond the Pickering emulsion example developed here in detail that can be directly realized experimentally, the results may provide fresh insight into other materials such as bijels[38, 39] that rely on such processes. A particularly exciting potential class of applications lies in biological matter, given the remarkable success in applying ideas from jamming to tissues and particularly tumor progression[5–8]. Future work should aim to integrate other developments from the jamming community, such as nonspherical particles and deformability[7, 12, 14, 19], to elucidate possible connections between the shape of the confining surface and particle shape. While the configurations observed here were hyperstatic, the nontrivial coupling of surface and particle degrees of freedom, and the new kinds of deformation mode that can emerge, foreshadows the recently identified need for more sophisticated approaches to characterizing rigidity[55]. Experimentally, the interplay of order and shape that emerges in metric jamming suggests the possibility of assembly processes that sculpt particulate media into a desired configuration by exploiting deformable interfaces; our framework provides a unified understanding to facilitate their design.

ACKNOWLEDGMENTS

We thank P. Spicer and A. Donev for helpful discussions. This material is based upon work supported by the National Science Foundation under Grant No. DMR-1654283.

MATERIALS & METHODS

Jammed configurations on fixed surfaces

We adapt the protocol for the generation of jammed configurations in 2D and 3D space[4] to packings on curved surface using the interparticle potential shown in Eq. (3). The simulation starts by randomly placing N particles of potentially different radii r_i with their centroids fixed on a curved surface that is scaled such that the area $A \gg N\pi r^2$ and hence the packing fraction $\phi \ll 1$. The simulation proceeds by iteratively reducing the size of the surface at fixed shape to slowly increase the packing fraction. Conjugate gradient descent is applied at each iteration to bring the particle interaction energy to the minimum; the sequence is terminated if the total potential energy per particle $V/N < 10^{-16}$ or V/N for successive iterations deviates by less than 10^{-15} . As the size of the surface decreases and the particles move closer to each other, inevitable overlaps appear and increase the energy minimum. The algorithm is halted if the minimized total potential energy per particle falls into $10^{-16} < V/N < 2 \times 10^{-16}$. This procedure brings the system extremely close to temperature $T = 0$, with a very small pressure $p < 10^{-10}$ as calculated below. These thresholds give a clear separation between jammed and unjammed state[42] and a similar approach has been utilized in other research about packings [40, 41, 47, 56, 57]. Packings are explicitly tested for rigidity by eigenanalysis as described in the main text.

Production of metric jammed configurations

We begin with a jammed packing on a fixed surface produces as described in the preceding section. Given such a configuration, described by parameters ξ , generalized forces are evaluated by taking the gradient of the energy functional (1), including the surface energy, with respect to the surface coefficients $\mathbf{f}_{c_{lm}} = -\nabla_{c_{lm}} E$. The surface is deformed along the descent direction with volume conservation by a stepsize δ and then the conjugate gradient method is employed to bring the particle system back to an energy minimum, as discussed above. The deformation is accepted if the total energy of the system afterwards is reduced, otherwise the deformation is rejected and the stepsize reduced $\delta \rightarrow \delta/2$. Further surface deformation steps are taken and the algorithm is stopped if $\delta < 10^{-16}$ or energy E for successive iterations deviates by less than 10^{-12} .

Calculation of mechanical properties

We calculate the stress tensor at each particle by constructing a local frame with tangent vectors \mathbf{t}_θ and \mathbf{t}_ϕ aligned in the polar and azimuthal directions respectively. The stress tensor in 2D[4, 44, 45, 57–59] is then written as,

$$\Sigma_{\alpha\beta} = \frac{1}{A} \sum_{i>j} (r_{ij\alpha} f_{ij\beta} + r_{ji\alpha} f_{ji\beta})/2, \quad (5)$$

where A is the surface energy and $r_{ij\alpha}$, $f_{ij\beta}$ represent the projections of center-to-center distance and force along surface tangent vectors \mathbf{t}_θ and \mathbf{t}_ϕ . The average is computed over pairs of particles. From this, we can com-

pute the pressure $p = (\Sigma_{\theta\theta} + \Sigma_{\phi\phi})/2$, bulk modulus $B = \psi dp/d\psi$ after slightly compressing the system at packing fraction ϕ and shear modulus $G = -d\Sigma_{\theta\phi}/d\gamma$ after applying a small shear strain γ [4, 44]. These variables are measured in units of k/r^2 where r is the radius of the larger particle. The shear is applied by twisting the configuration around the ellipsoid symmetry axis,

$$\psi_i = \begin{cases} \psi_i + 2\theta_i\gamma & 0 \leq \theta_i < \pi/2 \\ \psi_i + 2(\theta_i - \pi)\gamma & \pi/2 < \theta_i \leq \pi \end{cases}$$

after which we apply the conjugate gradient descent method to minimize the energy while fixing the position of several particles near the poles; these fixed particles and the area they cover are excluded from the stress tensor calculation.

-
- [1] M. van Hecke, *Journal of Physics: Condensed Matter*, 2009, **22**, 033101.
- [2] A. J. Liu and S. R. Nagel, *Annu. Rev. Condens. Matter Phys.*, 2010, **1**, 347–369.
- [3] A. J. Liu and S. R. Nagel, *Nature*, 1998, **396**, 21–22.
- [4] C. S. O’hern, L. E. Silbert, A. J. Liu and S. R. Nagel, *Physical Review E*, 2003, **68**, 011306.
- [5] D. Bi, J. Lopez, J. M. Schwarz and M. L. Manning, *Nature Physics*, 2015, **11**, 1074–1079.
- [6] D. Bi, X. Yang, M. C. Marchetti and M. L. Manning, *Physical Review X*, 2016, **6**, 021011.
- [7] S. Grosser, J. Lippoldt, L. Oswald, M. Merkel, D. M. Sussman, F. Renner, P. Gottheil, E. W. Morawetz, T. Fuhs, X. Xie *et al.*, *Physical Review X*, 2021, **11**, 011033.
- [8] L. Oswald, S. Grosser, D. M. Smith and J. A. Käs, *Journal of physics D: Applied physics*, 2017, **50**, 483001.
- [9] J. R. Stokes and W. J. Frith, *Soft Matter*, 2008, **4**, 1133–1140.
- [10] J. Mattsson, H. M. Wyss, A. Fernandez-Nieves, K. Miyazaki, Z. Hu, D. R. Reichman and D. A. Weitz, *Nature*, 2009, **462**, 83–86.
- [11] D. Vlassopoulos and M. Cloitre, *Current opinion in colloid & interface science*, 2014, **19**, 561–574.
- [12] K. VanderWerf, W. Jin, M. D. Shattuck and C. S. O’Hern, *Physical Review E*, 2018, **97**, 012909.
- [13] Y. Yuan, K. VanderWerf, M. D. Shattuck and C. S. O’Hern, *Soft matter*, 2019, **15**, 9751–9761.
- [14] J. D. Treado, D. Wang, A. Boromand, M. P. Murrell, M. D. Shattuck and C. S. O’Hern, *Physical Review Materials*, 2021, **5**, 055605.
- [15] D. Wang, J. D. Treado, A. Boromand, B. Norwick, M. P. Murrell, M. D. Shattuck and C. S. O’Hern, *Soft Matter*, 2021, **17**, 9901–9915.
- [16] D. Bi, J. Zhang, B. Chakraborty and R. P. Behringer, *Nature*, 2011, **480**, 355–358.
- [17] S. Henkes, D. A. Quint, Y. Fily and J. M. Schwarz, *Physical review letters*, 2016, **116**, 028301.
- [18] S. Papanikolaou, C. S. O’Hern and M. D. Shattuck, *Physical review letters*, 2013, **110**, 198002.
- [19] C. Brito, H. Ikeda, P. Urbani, M. Wyart and F. Zamponi, *Proceedings of the National Academy of Sciences*, 2018, **115**, 11736–11741.
- [20] M. Wyart, S. R. Nagel and T. A. Witten, *EPL (Europhysics Letters)*, 2005, **72**, 486.
- [21] M. Wyart, L. E. Silbert, S. R. Nagel and T. A. Witten, *Physical Review E*, 2005, **72**, 051306.
- [22] P. Charbonneau, E. I. Corwin, G. Parisi, A. Poncet and F. Zamponi, *Physical review letters*, 2016, **117**, 045503.
- [23] A. Ghosh, V. K. Chikkadi, P. Schall, J. Kurchan and D. Bonn, *Physical review letters*, 2010, **104**, 248305.
- [24] K. Chen, W. G. Ellenbroek, Z. Zhang, D. T. Chen, P. J. Yunker, S. Henkes, C. Brito, O. Dauchot, W. Van Saarloos, A. J. Liu *et al.*, *Physical review letters*, 2010, **105**, 025501.
- [25] L. E. Silbert, A. J. Liu and S. R. Nagel, *Physical review letters*, 2005, **95**, 098301.
- [26] L. E. Silbert, A. J. Liu and S. R. Nagel, *Physical Review E*, 2009, **79**, 021308.
- [27] E. DeGiuli, A. Laversanne-Finot, G. Düring, E. Lerner and M. Wyart, *Soft Matter*, 2014, **10**, 5628–5644.
- [28] M. L. Manning and A. J. Liu, *EPL (Europhysics Letters)*, 2015, **109**, 36002.
- [29] F. Arceri and E. I. Corwin, *Physical Review Letters*, 2020, **124**, 238002.
- [30] S. Torquato and F. H. Stillinger, *Reviews of modern physics*, 2010, **82**, 2633.
- [31] A. Donev, S. Torquato, F. H. Stillinger and R. Connelly, *Journal of applied physics*, 2004, **95**, 989–999.
- [32] A. Donev, S. Torquato, F. H. Stillinger and R. Connelly, *Journal of Computational Physics*, 2004, **197**, 139–166.
- [33] S. Torquato and F. H. Stillinger, *The Journal of Physical Chemistry B*, 2001, **105**, 11849–11853.
- [34] A. B. Pawar, M. Caggioni, R. Ergun, R. W. Hartel and P. T. Spicer, *Soft Matter*, 2011, **7**, 7710–7716.
- [35] A. Mikkelsen and Z. Rozynek, *ACS applied materials & interfaces*, 2019, **11**, 29396–29407.
- [36] A. L. Rodarte, R. J. Pandolfi, S. Ghosh and L. S. Hirst, *Journal of Materials Chemistry C*, 2013, **1**, 5527–7.
- [37] L. S. Dorobantu, A. K. Yeung, J. M. Foght and M. R. Gray, *Applied and environmental microbiology*, 2004, **70**, 6333–6336.
- [38] K. Stratford, R. Adhikari, I. Pagonabarraga, J.-C. Desplat and M. E. Cates, *Science*, 2005, **309**, 2198–2201.

- [39] E. M. Herzig, K. A. White, A. B. Schofield, W. C. Poon and P. S. Clegg, *Nature materials*, 2007, **6**, 966–971.
- [40] G.-J. Gao, J. Bławdziewicz and C. S. O’Hern, *Physical Review E*, 2006, **74**, 061304.
- [41] N. Xu, J. Bławdziewicz and C. S. O’Hern, *Physical Review E*, 2005, **71**, 061306.
- [42] D. Vågberg, P. Olsson and S. Teitel, *Physical Review E*, 2011, **83**, 031307.
- [43] C. P. Goodrich, A. J. Liu and S. R. Nagel, *Physical review letters*, 2012, **109**, 095704.
- [44] S. Chen, T. Bertrand, W. Jin, M. D. Shattuck and C. S. O’Hern, *Physical Review E*, 2018, **98**, 042906.
- [45] A. Boromand, A. Signoriello, J. Lowensohn, C. S. Orellana, E. R. Weeks, F. Ye, M. D. Shattuck and C. S. O’Hern, *Soft matter*, 2019, **15**, 5854–5865.
- [46] W. Helfrich, *Zeitschrift für Naturforschung C*, 1973, **28**, 693–703.
- [47] N. Xu, V. Vitelli, A. J. Liu and S. R. Nagel, *EPL (Europhysics Letters)*, 2010, **90**, 56001.
- [48] K. VanderWerf, A. Boromand, M. D. Shattuck and C. S. O’Hern, *Physical Review Letters*, 2020, **124**, 038004.
- [49] C. P. Goodrich, S. Dagois-Bohy, B. P. Tighe, M. van Hecke, A. J. Liu and S. R. Nagel, *Physical Review E*, 2014, **90**, 022138.
- [50] H. Mizuno, H. Shiba and A. Ikeda, *Proceedings of the National Academy of Sciences*, 2017, **114**, E9767–E9774.
- [51] L. Wang, A. Ninarello, P. Guan, L. Berthier, G. Szamel and E. Flenner, *Nature communications*, 2019, **10**, 1–7.
- [52] P. Debye, *Annalen der Physik*, 1912, **344**, 789–839.
- [53] R. Zeller and R. Pohl, *Physical Review B*, 1971, **4**, 2029.
- [54] Z. Zeravcic, W. van Saarloos and D. R. Nelson, *EPL (Europhysics Letters)*, 2008, **83**, 44001.
- [55] O. K. Damavandi, V. F. Hagh, C. D. Santangelo and M. L. Manning, *arXiv preprint arXiv:2102.11310*, 2021.
- [56] M. Mailman, C. F. Schreck, C. S. O’Hern and B. Chakraborty, *Physical review letters*, 2009, **102**, 255501.
- [57] C. F. Schreck, N. Xu and C. S. O’Hern, *Soft Matter*, 2010, **6**, 2960–2969.
- [58] M. P. Allen and D. J. Tildesley, *Computer simulation of liquids*, Oxford university press, 2017.
- [59] C. P. Goodrich, A. J. Liu and J. Sethna, *Proceedings of the National Academy of Sciences*, 2016, **113**, 9745–9750.